Mott Transition in a Metallic Liquid: Gutzwiller Molecular Dynamics Simulations

Gia-Wei Chern,[1,2,3] Kipton Barros,[1,2] Cristian D. Batista,[1,2] Joel D. Kress,[1] and Gabriel Kotliar[4]
[1]Theoretical Division, Los Alamos National Laboratory, Los Alamos, New Mexico 87545, USA
[2]Center for Nonlinear Studies, Los Alamos National Laboratory, Los Alamos, New Mexico 87545, USA
[3]Department of Physics, University of Virginia, Charlottesville, Virginia 22904, USA
[4]Department of Physics and Astronomy, Rutgers University, Piscataway, New Jersey 08854-8019, USA
(Received 16 September 2015; revised manuscript received 18 December 2015; published 1 June 2017)

We present a formulation of quantum molecular dynamics that includes electron correlation effects via the Gutzwiller method. Our new scheme enables the study of the dynamical behavior of atoms and molecules with strong electron interactions. The Gutzwiller approach goes beyond the conventional mean-field treatment of the intra-atomic electron repulsion and captures crucial correlation effects such as band narrowing and electron localization. We use Gutzwiller quantum molecular dynamics to investigate the Mott transition in the liquid phase of a single-band metal and uncover intriguing structural and transport properties of the atoms.

DOI: 10.1103/PhysRevLett.118.226401

The physics of Mott Hubbard correlations has been intensely studied because of its conceptual relevance to many classes of correlated materials. Previous studies have largely assumed fixed atom positions [1]. To understand correlated electron physics within metallic liquids, it is imperative to include correlation effects also on the atomic dynamics. In this Letter we incorporate the Gutzwiller method into quantum molecular dynamics (QMD) to elucidate the basic questions of how proximity to the Mott transition affects correlation functions of the liquid and how it impacts ionic and electronic transport.

The Gutzwiller variational wave function, together with the Gutzwiller approximation (GA) [2–4] provide an efficient approach to correlated materials. The basic idea is to apply an operator to a Slater determinant, which reduces the probability amplitude of doubly occupied states. The optimum double occupancy probability is determined variationally. As in the mean-field approach, the GA retains the desirable feature of an effective single-particle picture. More importantly, it captures crucial correlation effects, such as bandwidth renormalization. For instance, the Brinkman-Rice theory of the Hubbard model [5], which provided one of the first important steps towards our understanding of the Mott transition (MT), is based on the GA. Subsequently, the GA has been reformulated as the saddle point solution of a slave boson theory, leading to multiple generalizations and broadened applicability [6]. Moreover, the GA can be combined with density functional theory (DFT) [7,8]. Indeed, the local density approximation combined with the GA has proven to be a powerful scheme for studying real correlated metals [9–15].

It is well known that strong intra-atomic Coulomb interaction (U) induces electronic localization, which can trigger iso-structural transitions with large volume collapse in f-electron *lattice systems*, such as metallic Ce and Pu [9,16–20]. Similarly, we expect that the corresponding Mott-Anderson transition in correlated *liquid metals* will induce drastic changes in static and transport properties. Our Gutzwiller QMD (GQMD) scheme elucidates the U dependence of *both* the electronic and ionic transport coefficients. Specifically we develop a tight-binding (TB) QMD simulation coupled to a robust Gutzwiller solver. Tight binding is much faster, although less accurate, than full DFT-based MD [21]. We demonstrate our approach by investigating the effect of intra-atomic Coulomb repulsion on the structural and dynamical properties of the simplest possible model Hamiltonian, which describes a narrow s-band liquid metal. Besides the large volume expansion, we find that the strongly first order metal-insulator transition is accompanied by a drastic drop of the ionic self-diffusion coefficient.

We consider single-orbital atoms with an on-site Hubbard interaction U in a tight-binding formulation:

$$\mathcal{H}_e = \sum_{i\neq j}\sum_{\sigma} t(|\mathbf{r}_i-\mathbf{r}_j|)c^{\dagger}_{i,\sigma}c_{j,\sigma} + U\sum_i n_{i,\uparrow}n_{i,\downarrow} + \frac{1}{2}\sum_{i\neq j}\phi(|\mathbf{r}_i-\mathbf{r}_j|) + \sum_i \frac{|\mathbf{p}_i|^2}{2m}. \quad (1)$$

The first term is the electron hopping between neighboring atoms. The operator $c^{\dagger}_{i,\sigma}$ creates an electron with spin $\sigma=\uparrow,\downarrow$ at the ith atom. $n_{i,\sigma}=c^{\dagger}_{i,\sigma}c_{i,\sigma}$ is the electron number operator and $\mathbf{r}_i$ is the position vector of ith atom. $\phi(r)$ is the pairwise repulsive interatomic potential. The last term of (1) is the atomic kinetic energy (m and $\mathbf{p}_i$ are the atomic mass and momentum, respectively). For simplicity, we assume that both the hopping and pair-potential scale exponentially with the interatomic distance: $t(r)=t_0\exp(-r/\xi_1)$ and $\phi(r)=\phi_0\exp(-r/\xi_2)$. In applications to real materials, these parameters are usually determined

by fitting to bulk band-structure *ab initio* calculations or to experimental results [22]. Our scheme does not depend on details of this parametrization.

To efficiently include correlation effects induced by U, we adopt the GA and obtain the optimum many-electron wave function *at each time step* of the MD simulation. The optimized wave function depends only on the instantaneous ionic configuration when we adopt the Born-Oppenheimer approximation. Specifically, the ionic configuration $\{\mathbf{r}_i\}$ at each time step determines a tight-binding model parametrized by hopping amplitudes $t_{ij} = t(|\mathbf{r}_i - \mathbf{r}_j|)$. A Slater determinant $|\Psi_0\rangle$ is obtained from the single-particle eigenstates of the TB Hamiltonian. The correlated many-electron wave function is approximated by $|\Psi_G\rangle = \prod_i \mathcal{P}_i |\Psi_0\rangle$, where $\mathcal{P}_i$ is the Gutzwiller operator. Within the GA, which is exact in the infinite dimension limit, the expectation value of the off-site term acquires a renormalization: $\langle\Psi_G|c^\dagger_{i,\sigma}c_{j,\sigma}|\Psi_G\rangle = \mathcal{R}_{i,\sigma}\mathcal{R}_{j,\sigma}\langle\Psi_0|c^\dagger_{i,\sigma}c_{j,\sigma}|\Psi_0\rangle$, where

$$\mathcal{R}_{i,\sigma} = \frac{\sqrt{(1-\rho_{ii}+d_i)(\rho_{ii,\sigma}-d_i)} + \sqrt{d_i(\rho_{ii,\bar{\sigma}}-d_i)}}{\sqrt{\rho_{ii,\sigma}(1-\rho_{ii,\sigma})}}. \quad (2)$$

Here $\rho_{ij,\sigma} = \langle\Psi_0|c^\dagger_{i,\sigma}c_{j,\sigma}|\Psi_0\rangle$ is the single-particle density matrix, $\rho_{ii} = \rho_{ii,\uparrow} + \rho_{ii,\downarrow}$, and $d_i = \langle\Psi_G|n_{i,\uparrow}n_{i,\downarrow}|\Psi_G\rangle$ is the double occupancy probability at ith atom. The $\{d_i\}$ variables are treated as variational parameters to be determined by minimizing the Gutzwiller energy functional,

$$E_G = \frac{1}{2}\sum_{i\neq j}\sum_{\sigma} t_{ij}\mathcal{R}_{i,\sigma}\mathcal{R}_{j,\sigma}\rho_{ij,\sigma} + U\sum_i d_i. \quad (3)$$

Since we are interested in the high-temperature (T) liquid regime of $\mathcal{H}_e$, we employ a finite-T extension of the GA developed in Ref. [23]. The entropy correction due to the Gutzwiller operator is approximated by the lower bound $\Delta S = \ln\langle\Psi_0|\mathcal{P}|\Psi_0\rangle$. Since this variational correction ΔS is not a microscopic expression, this approach leads to an unphysical negative low-T entropy [23]. Nonetheless it gives a good approximation in the high-T regime of interest. More importantly, the inclusion of this entropy correction for a half-filled Hubbard model on a lattice reproduces the critical endpoint of the first order metal-insulator transition line obtained with DMFT [23]. Within this finite-T extension of the GA, the variational parameters $\{d_i\}$ are obtained by minimizing the total free energy:

$$F_G = -k_B T \ln \mathrm{Tr} e^{-\tilde{\beta}H_{\mathrm{TB}}} - \sum_i \left(e_i \ln\frac{e_i}{e_{i0}} + q_i \ln\frac{q_i}{q_{i0}} + d_i \ln\frac{d_i}{d_{i0}} \right), \quad (4)$$

where e_i and q_i are the empty and single-occupancy probabilities, and the subscript 0 denotes the probabilities for the uncorrelated wave function. The first term is the free energy of noninteracting fermions, whose TB Hamiltonian is renormalized by $\mathcal{R}_{i,\sigma}$. The second term arises from the correction ΔS of the Gutzwiller operators. Per the Born-Oppenheimer approximation, we assume the electrons are always in thermal equilibrium. Because strong correlations can produce a drastic suppression of the effective Fermi temperature, a strongly temperature dependent free energy functional is essential for describing correlated electronic degrees of freedom with MD [24].

In modern implementations of the GA, both the Slater determinant $|\Psi_0\rangle$ and the variational parameters $\{d_i\}$ are to be optimized through iterations [25]. The optimization of $|\Psi_0\rangle$ corresponds to solving the single-particle density matrix $\rho_{ij,\sigma}$ of the renormalized TB Hamiltonian $\tilde{H}_{\mathrm{TB}}$, while the parameters $\{d_i\}$ are obtained by minimizing F_G. In our implementation of the GQMD, these two optimizations are repeated until the iterations converge. An important criterion for convergence is to verify the constraint $\langle\Psi_G|n_{i,\sigma}|\Psi_G\rangle = \langle\Psi_0|n_{i,\sigma}|\Psi_0\rangle$. Once the optimal solution is obtained, we compute the forces acting on the ions,

$$\mathbf{f}_i = -\sum_{j,\sigma}\frac{\partial t(r_{ij})}{\partial \mathbf{r}_i}\mathcal{R}_{i,\sigma}\mathcal{R}_{j,\sigma}\rho_{ij,\sigma} - \sum_j \frac{\partial \phi(r_{ij})}{\partial \mathbf{r}_i}. \quad (5)$$

Given the forces, we integrate the ionic positions one time step using the velocity Verlet method with Langevin noises [26].

We now apply the GQMD to simulate the liquid phase of an s-band system, such as hydrogen at high temperatures. Since our main interest is the MT in the paramagnetic phase, we restrict ourselves to nonmagnetic solutions. We use a constant volume V and constant temperature MD simulation with $N = 100$ atoms. Periodic boundary conditions are used in all simulations. The temperature T is kept constant by using a Langevin thermostat [26] with a rather small damping $\gamma \sim 10^{-3}$–10^{-2} fs^{-1}. V is determined from the average interatomic distance $r_s = (3V/4\pi N)^{1/3} \approx 1.6 r_0$, where r_0 is the equilibrium distance between two atoms in the molecular state (e.g., H_2). Here we will only consider the half-filled case with a number of electrons $N_e = N$. The atoms are randomly distributed within the simulation box at the beginning of the simulation, and the system relaxes to equilibrium in a few thousands MD steps. The time step is 0.5 fs and the total trajectory simulations are of order 10^7 fs. Our Gutzwiller solver is rather efficient; it takes an average of less than 10 iterations to reach convergence in equilibrium, but the number of iterations can be as high as a few hundreds during the relaxation process. We have adopted a recently proposed efficient implementation of the Gutzwiller solver [25], in which the minimization of F_G is recast into an eigenvalue problem. This new formulation also provides the advantage of

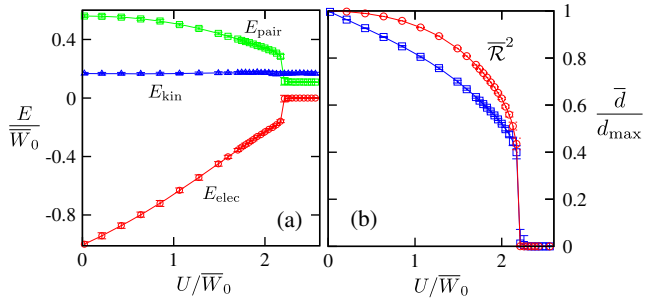

FIG. 1. (a) Average electronic energy $E_{\rm elec}$, pair-potential $E_{\rm pair}$, and kinetic energy $E_{\rm kin}$ as a function of U. The roughly constant kinetic energy is determined from the simulation temperature (not affected by U). (b) Average double occupancy $\bar{d}/d_{\rm max}$ and renormalization $\bar{\mathcal{R}}^2$ as a function of U. The maximum double occupancy is $d_{\rm max} = \langle n_\uparrow \rangle \langle n_\downarrow \rangle = 0.25$.

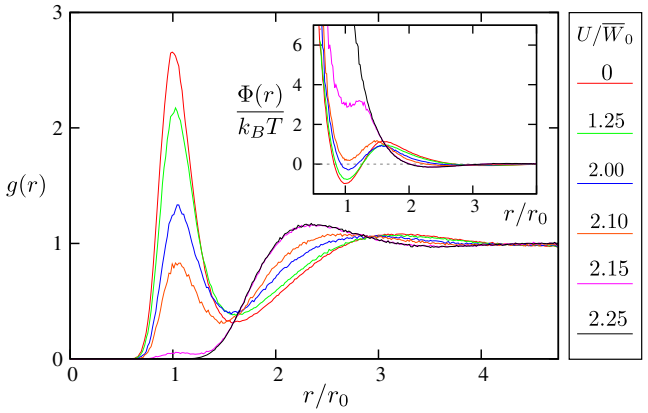

FIG. 2. Pair distribution function $g(r)$ obtained from GQMD for varying values of U. Here d is the equilibrium distance between atoms in a molecule. The explicit value of r_0 is determined by the minimum of the energy curve $e(r) = -2t(r) + \phi(r)$. The simulation temperature is $k_B T \sim 0.1\bar{W}_0$. The inset shows the potential of mean force $\Phi(r) = -k_B T \ln g(r)$.

numerical stability and can be systematically generalized to multiorbital systems.

Figure 1(a) shows the electron, pair potential, and kinetic energy as a function of U. All the energies are normalized to the average band energy $\bar{W}_0$. The energy scale $\bar{W}_0 = \langle |E_{\rm elec}| \rangle_{U=0}$ provides a measure of the intrinsic bandwidth of the system, and is obtained by averaging the electronic energy at zero Hubbard U. In equilibrium, the Langevin thermostat ensures that the kinetic energy per atom satisfies $E_{\rm kin} = \frac{3}{2} k_B T$. Both the electronic energy $E_{\rm elec}$ and the pair-potential $E_{\rm pair}$ show a pronounced change at a critical value $U_c \approx 2.1\bar{W}_0$. The electronic energy here includes the binding energy of the TB Hamiltonian and the Hubbard interaction term. Above U_c, the electron energy vanishes identically indicating that the system enters a new phase with distinctly different electronic properties. The nature of this MT can be inferred from the U dependence of the average renormalization and the double-occupancy probability shown in Fig. 1(b). Here $\bar{R}^2$ is used as an estimate of the electron bandwidth renormalization. The averaged renormalization is close to one, $\bar{R}^2 \approx 1$, for $U \ll \bar{W}_0$ and it quickly decreases to zero for $U \gtrsim U_c$, indicating a first-order transition. The double occupancy remains close to the uncorrelated value, $\bar{d} \approx \langle n_\uparrow \rangle \langle n_\downarrow \rangle \approx 0.25$, for small U, while it vanishes above U_c. The renormalization to zero of the effective bandwidth shows that the metal-insulator transition is driven by electronic localization, as also evidenced by the vanishing double occupation for $U > U_c$.

The radial pair distribution function $g(r)$ is the probability of finding an atom at a distance r from a reference atom [26]. At small U, the $g(r)$ curves obtained from our GQMD simulations exhibit a pronounced peak at the equilibrium distance r_0 of the binding energy $e(r) = -2t(r) + \phi(r)$ (see Fig. 2). This peak arises from the formation of quasidimer molecules in the liquid phase [27,28]. As U increases, the dimer peak gradually disappears, while the second broader peak moves toward longer distances. The trend is consistent with the MT scenario in which increasing Coulomb repulsion suppresses the formation of a covalent bond as electrons become localized. The molecular peak disappears above $U = U_c \simeq 2.1\bar{W}_0$ and the distribution function only exhibits a broad peak at $r \sim 2.2 r_0$.

The metal-insulator transition is also demonstrated by the U dependence of the dc conductivity σ [Fig. 3(a)] computed with the Kubo-Greenwood formula [29,30]. The current operator has a simple form in the tight-binding basis [31]. While σ vanishes above U_c, the sharp increase when U approaches U_c from the metallic side is caused by the dimer dissociation, which is accelerated near the MT (see Fig. 2). Similar to the case of doped semiconductors, each isolated atom (or monomer) introduces an electronic state inside the bonding-antibonding gap of the dimer spectrum [32,33]. According to Mott's approximation [34], σ is proportional to the square of the density of states at the Fermi level, implying that it should also be proportional to the square of the monomer density ρ_m, as illustrated in a previous work [32]. The linear increase of ρ_m with U for $1 \lesssim U/\bar{W}_0 \lesssim 2$ explains the quadratic increase of $\sigma(U)$ in the same interval. The combination of this effect with the rapid suppression of σ at the MT leads to the rather sharp peak at U_c.

The histogram of double-occupancy probability $h(d)$ shown in Fig. 3(b) exhibits an interesting bimodal distribution when U approaches U_c. The two peaks of this bimodal distribution arise from the dissociation of dimers into monomers. The sharper dimer peak is always centered around higher $d/d_{\rm max}$ values because the hopping amplitude between the two atoms in a dimer is clearly larger than the average hopping amplitude between monomers. The monomer peak is much broader because of the broader distribution of monomer-monomer and monomer-dimer distances relative to the distribution distances between two ions in the same dimer.

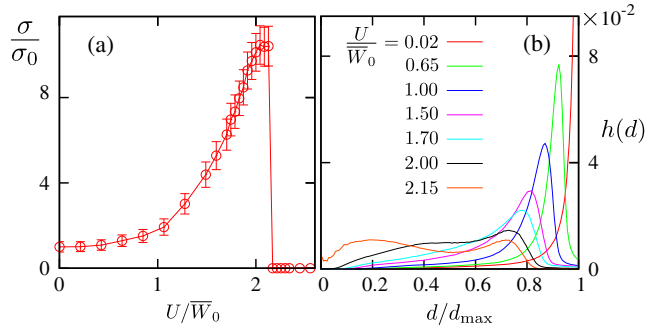

FIG. 3. (a) dc conductivity σ normalized to the value at $U = 0$ as a function of U. (b) Distribution of the double-occupancy probability d for different U values. The simulation temperature is $k_B T \sim 0.1\bar{W}_0$.

The coefficient of self-diffusion is an important measure of the dynamics of the liquid phase. It is computed from the velocity autocorrelation function [26],

$$D = \frac{1}{3N} \sum_i \int_0^\infty \langle \mathbf{v}_i(t) \cdot \mathbf{v}_i(0) \rangle dt.$$

Figure 4 shows the normalized self-diffusion coefficient obtained from our GQMD simulations. The original increase of $D(U)$ is related to the suppression of the molecular peak in $g(r)$. At small U, the atoms form transient bound dimers, whose larger effective mass leads to smaller D values. In parallel, the simultaneous change of the effective two-atom potential for increasing U modifies the self-diffusion coefficient of the increasing number of monomers. To demonstrate that this effect leads to the drastic drop of D at U_c, we compute the Chapman-Enskog self-diffusion coefficient to first order [35],

$$[D]_1 = \frac{3}{8} \sqrt{\frac{\pi k_B T}{m}} \left(\frac{1}{n \Omega^{(1,1)}} \right), \tag{6}$$

where n is the density and $\Omega^{(1,1)}$ is the collision integral for diffusion obtained from the effective two-atom potential of mean force $\Phi(r) = -k_B T \ln g(r)$ shown in the inset of Fig. 2. $\Phi(r)$ includes correlation effects self-consistently [36,37]. In general, the effect of integrating out the electrons cannot be reduced to a simple two-body effective interaction. Nevertheless, because the coupling to the electronic degrees of freedom weakens near the MT ($\bar{R}^2$ is strongly suppressed), we expect that the effective two-body potential provides a reasonable description in this "weak-coupling" regime. Indeed, the result shown in the inset of Fig. 4 agrees quite well with the self-diffusion coefficient directly obtained from the GQMD simulation near the MT. The same level of agreement is not obtained for small U values because the formation of molecular states is not accounted for in this simplified analysis.

This calculation shows that the nonmonotonic dependence of $D(U)$ arises from the change of $\Phi(r)$ with U. $\Phi(r)$ is strongly attractive around $r \sim r_0$ for small U values due

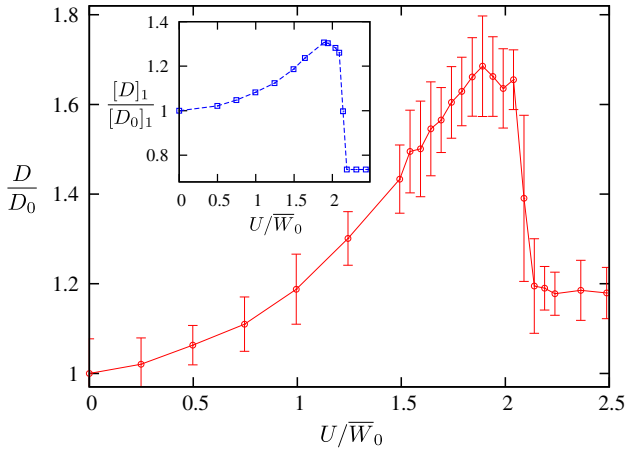

FIG. 4. Self-diffusion coefficient D as a function of U. D_0 is the diffusion constant for $U = 0$. The simulation temperature is $k_B T \sim 0.1\bar{W}_0$. The inset shows the same self-diffusion coefficient, $[D]_1/[D_0]_1$, as approximated by the Chapman-Enskog theory for the effective potential $\Phi(r)$.

to a large electronic contribution (see inset of Fig. 2). The corresponding potential barrier at $r \simeq 1.5 r_0$ increases the transport cross section in the energy range $E \lesssim k_B T$ most relevant for the collision integral. The height of this barrier decreases with U because the attractive electronic component becomes weaker. The resulting suppression of the transport cross section explains the corresponding increase of $D(U)$ shown in the inset of Fig. 4. This behavior changes drastically for $U \gtrsim U_c$ because of the discontinuous suppression of the electronic binding energy. In this regime, the atoms interact only via the potential $\phi(r)$. The resulting transport cross section is similar to the $U = 0$ case for $E \lesssim k_B T$ and it is even higher for $E > k_B T$ (see inset of Fig. 2). This explains the drastic drop of D at the MT.

MD simulations are widely used to understand fundamental properties of materials such as molecular structures, transport, phase transitions, and chemical reactions. Full quantum mechanical treatment of electron wave functions has the potential to greatly increase the predictive power of MD [38]. For many functional materials, including transition metal and rare-earth compounds, electron correlation effects are known to be crucial, yet are neglected even in state-of-the-art MD simulations. Our implementation of the single-band case provides a proof of principle for including electron correlations in MD simulations. Although there are more accurate methods, e.g., MD combined with variational quantum Monte Carlo simulations [39–41] and path-integral QMD [42,43], for the single-band atoms such as hydrogen, the Gutzwiller MD scheme is the only method that can be feasibly generalized to multiorbital correlated materials of primary interest, such as d and f-electron systems, as demonstrated recently by calculations of the equation of state of Pr and Pu [44].

Recent developments can increase the efficiency of GQMD. A dominant computational cost of electronic structure solvers is calculating the density matrix from

the TB Hamiltonian. Direct diagonalization has computational cost that scales cubically with the system size. The kernel polynomial method (KPM) can provide stochastic estimates of the electronic free energy [45]. The gradient transformation of the KPM energy estimation procedure yields density matrix elements, as required by Gutzwiller, with computational cost that scales linearly with system size for both insulating and metallic systems [46,47]. Another future direction is generalizing the extended Lagrangian formalism [48,49] to the GQMD self-consistency equations. The integration of these techniques into the GQMD seems very promising.

We acknowledge useful discussions with A. Niklasson, Y. Motome, J.-P. Julien, and J.-X. Zhu. Work at LANL was carried out under the auspices of the U.S. DOE Contract No. DE-AC52-06NA25396 through the LDRD program. G. K. was supported by DOE BES DE-FG02-99ER45761. The numerical simulations were performed using the CCS-7 Darwin cluster at LANL. Software and algorithm development (C. D. B and G. W. C) was supported by the Center for Materials Theory as a part of the Computational Materials Science (CMS) program, funded by the U.S. Department of Energy, Office of Science, Basic Energy Sciences, Materials Sciences and Engineering Division.

[1] Exceptions include recent work to optimize the atomic orbitals in response to volume change, e.g., A. P. Kadzielawa, A. Bielas, M. Acquarone, A. Biborski, M. M. Maśka, and J. Spalek, New J. Phys. **16**, 123022 (2014).
[2] M. C. Gutzwiller, Phys. Rev. Lett. **10**, 159 (1963).
[3] M. C. Gutzwiller, Phys. Rev. **134**, A923 (1964).
[4] M. C. Gutzwiller, Phys. Rev. **137**, A1726 (1965).
[5] W. F. Brinkman and T. M. Rice, Phys. Rev. B **2**, 4302 (1970).
[6] G. Kotliar and A. E. Ruckenstein, Phys. Rev. Lett. **57**, 1362 (1986).
[7] P. Hohenberg and W. Kohn, Phys. Rev. **136**, B864 (1964).
[8] W. Kohn and L. J. Sham, Phys. Rev. **140**, A1133 (1965).
[9] N. Lanatá, Y.-Xin Yao, C.-Z. Wang, K.-M. Ho, and G. Kotliar, Phys. Rev. X **5**, 011008 (2015).
[10] J.-P. Julien and J. Bouchet, Prog. Theor. Chem. Phys. B **15**, 509 (2006).
[11] K. M. Ho, J. Schmalian, and C. Z. Wang, Phys. Rev. B **77**, 073101 (2008).
[12] X. Y. Deng, L. Wang, X. Dai, and Z. Fang, Phys. Rev. B **79**, 075114 (2009).
[13] J. Bünemann, F. Gebhard, T. Ohm, S. Weiser, and W. Weber, Phys. Rev. Lett. **101**, 236404 (2008).
[14] G. Borghi, M. Fabrizio, and E. Tosatti, Phys. Rev. B **90**, 125102 (2014).
[15] A recent GA-MD approach without self-consistent Gutzwiller iteration was applied to study 16 atoms close to equilibrium positions of a square lattice; see J.-P. Julien, J. D. Kress, and J.-X. Zhu, arXiv:1503.00933.
[16] Nicola Lanatá, Yong-Xin Yao, Cai-Zhuang Wang, Kai-Ming Ho, and Gabriel Kotliar, Phys. Rev. B **90**, 161104 (2014).
[17] Nicola Lanatá, Yongxin Yao, Cai-Zhuang Wang, Kai-Ming Ho, and Gabriel Kotliar, arXiv:1405.6934.
[18] J. W. Allen and R. M. Martin, Phys. Rev. Lett. **49**, 1106 (1982).
[19] M. Lavagna, C. Lacroix, and M. Cyrot, Phys. Lett. **90A**, 210 (1982).
[20] B. Johansson, Philos. Mag. **30**, 469 (1974).
[21] D. Marx and J. Hutter, in *Modern Methods and Algorithms of Quantum Chemistry*, 2nd ed., edited by J. Grotendorst (John von Neumann Institute for Computing Julich, Germany, 2000).
[22] I. Kwon, J. D. Kress, and L. A. Collins, Phys. Rev. B **50**, 9118 (1994).
[23] W.-S. Wang, X.-M. He, D. Wang, Q.-H. Wang, Z. D. Wang, and F. C. Zhang, Phys. Rev. B **82**, 125105 (2010).
[24] Z. P. Yin, Xiaoyu Deng, K. Basu, Q. Yin, and G. Kotliar, Philos. Mag. Lett. **94**, 620 (2014).
[25] N. Lanata, H. U. R. Strand, X. Dai, and B. Hellsing, Phys. Rev. B **85**, 035133 (2012).
[26] M. P. Allen and D. J. Tildesley, *Computer Simulation of Liquids* (Oxford Science, Oxford, England, 1987).
[27] L. Collins, I. Kwon, J. Kress, N. Troullier, and D. Lynch, Phys. Rev. E **52**, 6202 (1995).
[28] G. Mazzola, S. Yunoki, and S. Sorella, Nat. Commun. **5**, 3487 (2014).
[29] N. W. Ashcroft and N. D. Mermin, *Solid State Physics* (Saunders College, Philadelphia, 1976).
[30] M. P. Desjarlais, J. D. Kress, and L. A. Collins, Phys. Rev. E **66**, 025401(R) (2002).
[31] G. D. Mahan, *Many Particle Physics* (Kluwer Academics/ Plenum Publishers, New York, 2000).
[32] T. J. Lenosky, J. D. Kress, L. A. Collins, and I. Kwon, Phys. Rev. B **55**, R11907 (1997).
[33] M. Ross, Phys. Rev. B **54**, R9589 (1996).
[34] N. F. Mott and E. A. Davis, *Electronic Processes in Non-Crystalline Materials* (Calendon Press, Oxford, England, 1979), Chap. 1.
[35] S. Chapman and T. Cowling, *The Mathematical Theory of Non-Uniform Gases* (Cambridge University, Cambridge, England, 1970).
[36] J. G. Kirkwood, J. Chem. Phys. **3**, 300 (1935).
[37] S. D. Baalrud and J. Daligault, Phys. Rev. Lett. **110**, 235001 (2013).
[38] R. Car and M. Parrinello, Phys. Rev. Lett. **55**, 2471(1985).
[39] K. T. Delaney, C. Pierleoni, and D. M. Ceperley, Phys. Rev. Lett. **97**, 235702 (2006).
[40] C. Attaccalite and S. Sorella, Phys. Rev. Lett. **100**, 114501 (2008).
[41] N. M. Tubman, E. Liberatore, C. Pierleoni, M. Holzmann, and D. M. Ceperley, Phys. Rev. Lett. **115**, 045301 (2015).
[42] C. Pierleoni, D. M. Ceperley, B. Bernu, and W. R. Magro, Phys. Rev. Lett. **73**, 2145 (1994).
[43] W. R. Magro, D. M. Ceperley, C. Pierleoni, and B. Bernu, Phys. Rev. Lett. **76**, 1240 (1996).
[44] N. Lanatá, Y-X Yao, C-Z Wang, K-M Ho, and G. Kotliar, Phys. Rev. X **5**, 011008 (2015).
[45] A. Weiße, G. Wellein, A. Alvermann, and H. Fehske, Rev. Mod. Phys. **78**, 275 (2006).
[46] K. Barros and Y. Kato, Phys. Rev. B **88**, 235101 (2013).
[47] K. Barros, J. W. F. Venderbos, G.-W. Chern, and C. D. Batista, Phys. Rev. B **90**, 245119 (2014).
[48] A. M. N. Niklasson, Phys. Rev. Lett. **100**, 123004 (2008).
[49] M. J. Cawkwell and A. M. N. Niklasson, J. Chem. Phys. **137**, 134105 (2012).